24/phdap/14 BHARAT BHUSHAN

SYNOPSIS DIKSHA_

NFL

Document Details

Submission ID
trn:oid:::27535:141151906

Submission Date
May 31, 2026, 10:20 PM GMT+5:30

Download Date
May 31, 2026, 10:24 PM GMT+5:30

File Name
SYNOPSIS DIKSHA_.pdf

File Size
2.6 MB

31 Pages

7,653 Words

39,479 Characters

7% Overall Similarity

The combined total of all matches, including overlapping sources, for each database.

Filtered from the Report

- Bibliography
- Small Matches (less than 12 words)

Match Groups

28 Not Cited or Quoted 7%
Matches with neither in-text citation nor quotation marks

0 Missing Quotations 0%
Matches that are still very similar to source material

0 Missing Citation 0%
Matches that have quotation marks, but no in-text citation

0 Cited and Quoted 0%
Matches with in-text citation present, but no quotation marks

Top Sources

2% Internet sources
5% Publications
3% Submitted works (Student Papers)

Integrity Flags

0 Integrity Flags for Review

Our system's algorithms look deeply at a document for any inconsistencies that would set it apart from a normal submission. If we notice something strange, we flag it for you to review.

A Flag is not necessarily an indicator of a problem. However, we'd recommend you focus your attention there for further review.

Match Groups

- **28** Not Cited or Quoted 7%
  Matches with neither in-text citation nor quotation marks
- **0** Missing Quotations 0%
  Matches that are still very similar to source material
- **0** Missing Citation 0%
  Matches that have quotation marks, but no in-text citation
- **0** Cited and Quoted 0%
  Matches with in-text citation present, but no quotation marks

Top Sources

2% Internet sources
5% Publications
3% Submitted works (Student Papers)

Top Sources

The sources with the highest number of matches within the submission. Overlapping sources will not be displayed.

1	Publication	
Shikha Verma, Labhansh Chaurasia, Sheetal Kumari, Aman Prasad, A.S. Rao. "Red...		4%
2	Student papers	
Thapar University, Patiala on 2020-06-27		<1%
3	Internet	
escholarship.org		<1%
4	Internet	
sutir.sut.ac.th:8080		<1%
5	Student papers	
Anna University on 2024-12-23		<1%
6	Student papers	
Higher Education Commission Pakistan on 2020-03-12		<1%
7	Publication	
Seungon Jung, Yunseong Choi, Yujin Kim, Yunjeong Jang et al. "Strain Engineerin...		<1%
8	Student papers	
Thapar University, Patiala on 2019-06-20		<1%
9	Internet	
ijsrst.com		<1%
10	Student papers	
GGS IP University Delhi on 2020-10-01		<1%

11 Publication

Hongxia Guan, Ye Sheng, Yanhua Song, Chengyi Xu, Xiuqing Zhou, Keyan Zheng, ... <1%

12 Student papers

Indian Institute of Technology, Madras on 2017-05-09 <1%

13 Student papers

National Institute of Technology on 2025-04-14 <1%

14 Student papers

National Sun Yat-sen University on 2016-07-18 <1%

15 Internet

erepository.uonbi.ac.ke:8080 <1%

16 Internet

mdpi-res.com <1%

17 Internet

www.nature.com <1%

CHAPTER1

INTRODUCTION

1.1. LUMINESCENCE

The emission of light from living or dead animals, plants (such as fungi), and the aurora has always fascinated humans and sparked curiosity about its origin. This phenomenon is none other than luminescence. It refers to the emission of light, not due to heating, as seen in incandescent lamps, discovered by Thomas Edison in 1879. It was a great pioneering work for the study of light. The incandescent lamps were solely based on heating a thin metal filament, such as tungsten, with very high melting and vapor points, inside a glass bulb to very high temperatures (2700°C) via applied voltage, and cause the illumination by the heating of the filament [1].

However, his work was a great discovery at that time, but later it proved to be energy inefficient and had high operating costs. It was soon replaced by the now-known LEDs that are more user-friendly.

This phenomenon itself was an accidental discovery by an alchemist named Vincenzo Cascariolo in 1603 as he was heating a mineral compound of $BaSO_4$ to find gold, but ended up with a crystal that glows in the dark. He called this glowing material “Bolognian stone”. It will glow in the dark after being exposed to sunlight. This was an accident that led to the development of the now well-known major field of physics, “luminescence” [2].

(a) Beach Bioluminescence

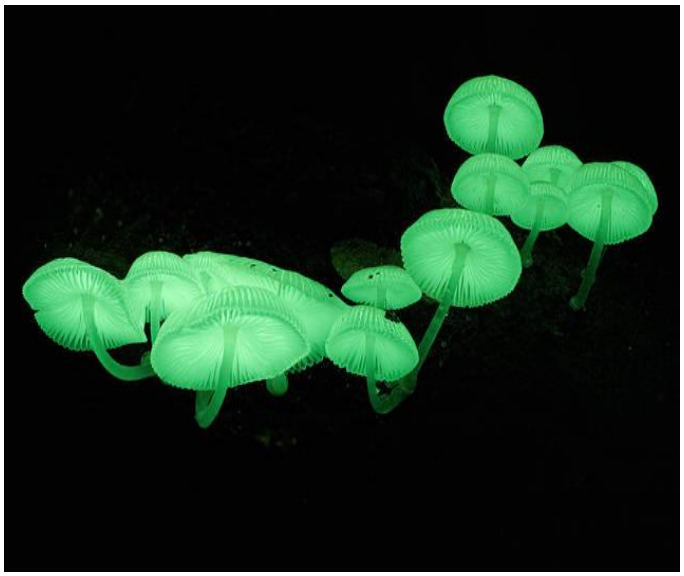

(b) Mycena chlorophos

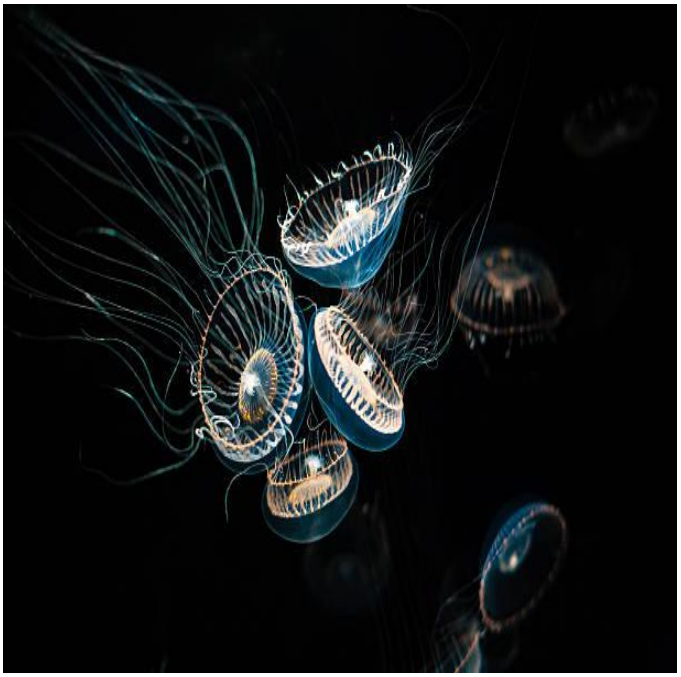

(c) Aequorea Victoria

(d) Glow fly

Figure 1.1: Luminescence in nature

Now there are different types of Luminescence:

a) Chemiluminescence (Excitation by Chemical Reaction)

b) Electroluminescence (Excitation by Electric Current/Field)

c) Radioluminescence (material is bombarded by high-energy radiation (X-rays, alpha, beta, gamma rays).

d) Mechanoluminescence (mechanical action on a solid, like crushing, rubbing, or scratching.

e) Photoluminescence (Excitation by Light)

1.2. PHOTOLUMINESCENCE

It's the phenomenon of emission of light from a material, but due to excitation of valence electrons in it and not due to heating, thus this is also called "cold light".

Under this category of Photoluminescence - the excitation by photons and then emission of a photon is further categorised based on their emission times :

a) Fluorescence

b) Phosphorescence

These phenomena have brilliant photon-emitting capabilities in the visible range upon illumination by photons of (UV-VIS-NIR), the only difference between them is in the time taken for the emission of the absorbed energy.

1.2.1 FLUORESCENCE

These materials are often called fluorophores; they are capable of absorbing photons in the UV-VIS-NIR region, which causes the material's electrons to get excited immediately, and then, as they lose their energy due to vibrations, they come back down to the ground state immediately. Thus, the time of the emission reaction is between 10^{-9} and 10^{-8} seconds. This implies that the reaction is almost spontaneous and that the emission lasts as long as the material is illuminated.

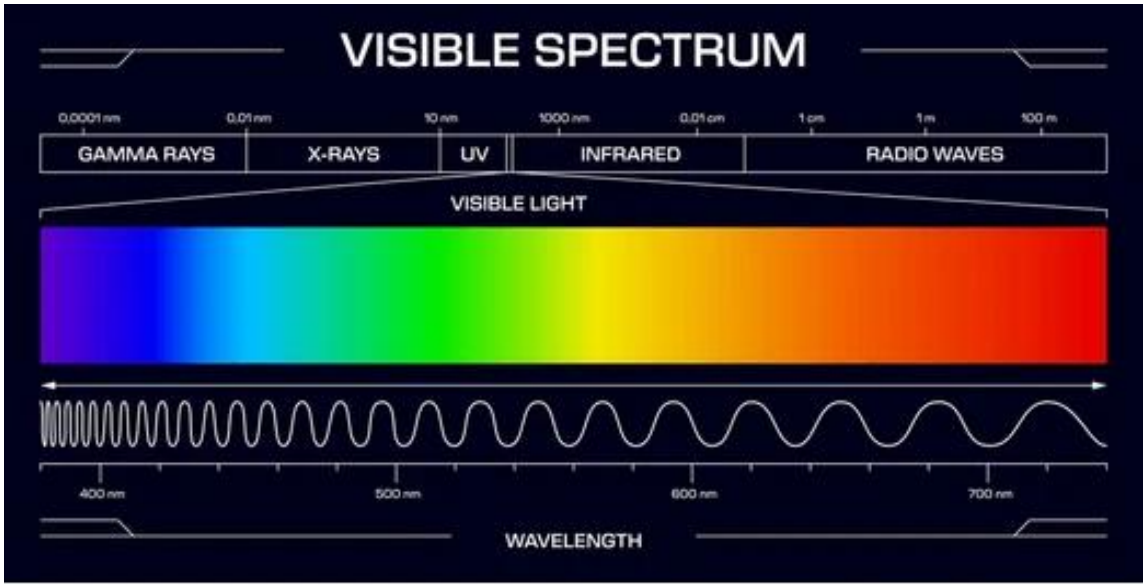

Figure 1.2: Electromagnetic Spectrum

1.2.2 PHOSPHORESCENCE

Materials that exhibit phosphorescence are called phosphors. These can absorb photons in the UV-VIS-NIR regions, thereby exciting their electrons, but instead of directly falling down from the excited state to the ground state, there is an intersystem crossing to a level that lies lower than the excited state but much higher than the ground state. This level attracts the excited electron as it falls back; here, spin inversion occurs, and the electron tends to remain longer in this state. The time for which an electron is in the state can range from a few minutes to hours. Thus, the material, once illuminated, can emit light for a longer period, with a delayed reaction time of 10^{-4} seconds.

Figure 1.3: Photoluminescent Material (glow in dark)

1.3. HOW PHOSPHOR MATERIALS ARE MADE

Phosphor luminescence occurs when an electron gains energy by absorbing the incident photons, but instead of coming back down to the ground state immediately, it wanders off, in a sense. It will first show us some intersystem crossing, or one might call it spin flipping, where the excited electron gets stuck in a triplet state. Now this triplet state is a kind of metastable state. It can trap the electron or hold it for milliseconds or hours; this results in delayed decay to the ground state. This means that if we start illuminating a phosphorescent material with UV rays right now, the excitation of valence electrons might occur immediately, but the emission will most likely occur after the illumination stops.

The main idea behind phosphorescent material is to be able to store enough energy for the excitation of the electrons and then the slow release of the energy. So, we synthesise it by taking a host, usually crystalline, and doping it with rare-earth elements. Thus, the material's physical nature is related to its chemical role.

The elements from atomic no. 57 to 71, along with scandium and yttrium, are called rare earth elements or lanthanide elements. They are usually used as dopants to introduce the impurity in the crystal lattice of the host in the required amount. These dopant elements are called activators or active centers, which provide the characteristic feature to the phosphor materials to absorb UV-VIS-NIR photons and then emit photons in the visible range[3].

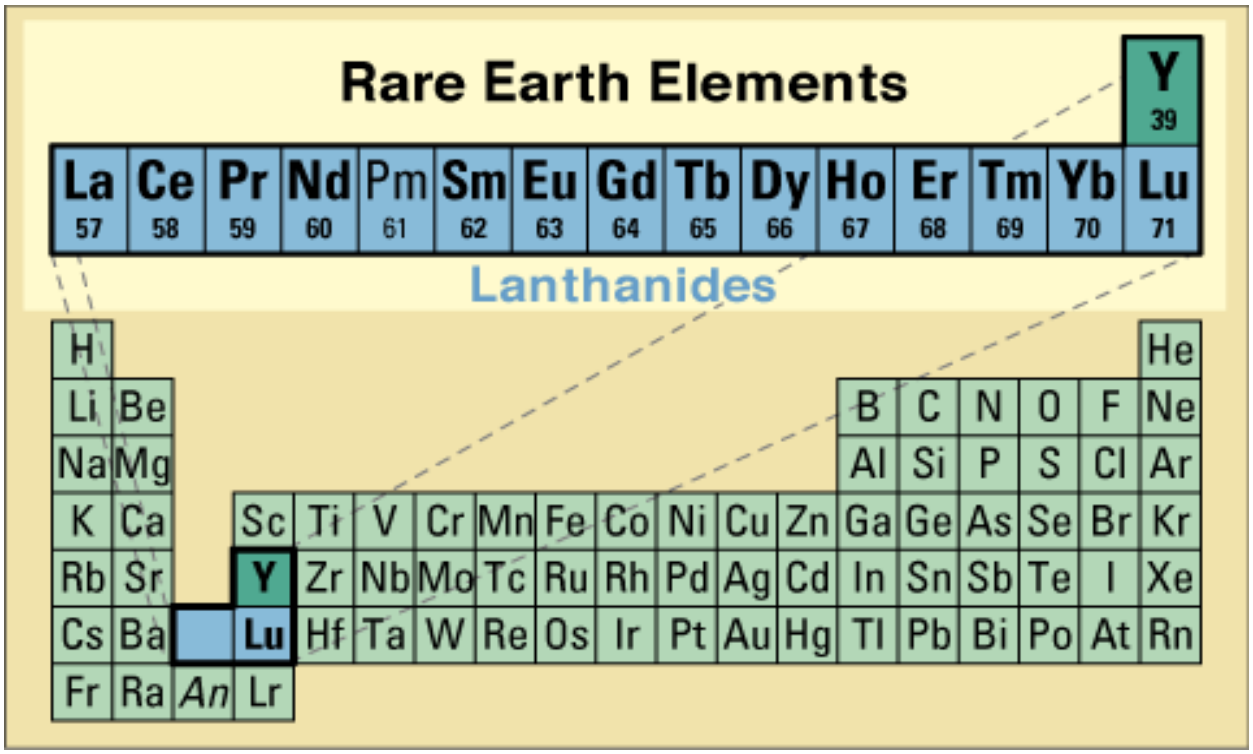

Figure 1.4: Rare Earth Elements

The host material can be any of oxides, aluminates, silicates, sulphides, tungstates, alumino-silicates, and nitrides or a mixture of these. Here, for our sample $Ba_3SrNb_2O_9$, we have used Barium carbonate ($BaCO_3$),

Strontium carbonate ($SrCO_3$), and Niobate Penta-Oxide (Nb_2O_5). We mixed these materials to achieve homogeneity, then the dopant is added with a rare earth element, like here, Europium (Eu^{3+})[4].

1.4. DIFFERENT PHOSPHOR MATERIAL SYNTHESIS METHODS

Phosphor luminescent materials exhibit different spectral emissions and properties depending on their dopant and particle size, which can affect and help determine their applications. There are a few different techniques to synthesise these materials, such as (i) the sol-gel technique, (ii) the solution combustion, and (iii) the solid-state synthesis. All these different synthesis methods yield particles of different sizes.

1.4.1 SOL-GEL TECHNIQUE

The material is first made into a homogenous solution and then, through numerous hydrolysis and condensation processes, is reduced to a gel formation. Then there occur different processes such as calcination (heat treatment), ageing and drying to make the final product more resilient, such as ceramics. The particle size is usually in the range of 5 nm - 200 nm.

Solution combustion:

It uses an organic compound and a metal nitride that will result in the metallic host for the phosphor materials. The metal nitride is mixed with the distilled water to form a homogenous solution, and then the organic compounds are added in a specific ratio as a fuel, such that the best combustion efficiency is reached. This material is added on a heated plate of about 400-500 degrees Celsius, where it evaporates immediately and results in a gel-like formation. Now, this gel is further heated, and the material undergoes a self-sustained redox reaction. It is a very short reaction, as this auto-combustion happens immediately and results in the final product as ash.

1.4.2 SOLID STATE SYNTHESIS

The material is synthesised using hand grinding or other techniques, with acetone added at regular intervals, and then further processed on different temperature profiles to achieve the final product. The particle size is quite bigger in this case, ranging from 1 to 10 μm.

1.5. HOW THE EMISSION OF LIGHT OCCURS

There are three major events in the light emission of phosphor materials. The first and foremost is the illumination of the material with UV-VIS-NIR radiation to excite the electrons; this is called the excitation of the material. After excitation, there occur internal relaxations or intersystem transitions, and the electron reaches a triplet state where the electrons are virtually trapped, and the spin flip occurs. The material in the singlet state is said to be anti-parallel in spins, and those in the triplet state are parallel spins. As the spins become parallel to each other, the distance between the electrons increases to attain stability in that state,

thus providing its characteristic nature of being meta-stable and being able to hold off the electrons for quite longer durations before it can go back to its original state, and emission of photons in the visible range can occur. This allows the material to emit photons and for the electrons to return to their ground state after a period of time, thereby causing delayed emission of photons or light and completing the phosphorescence process.

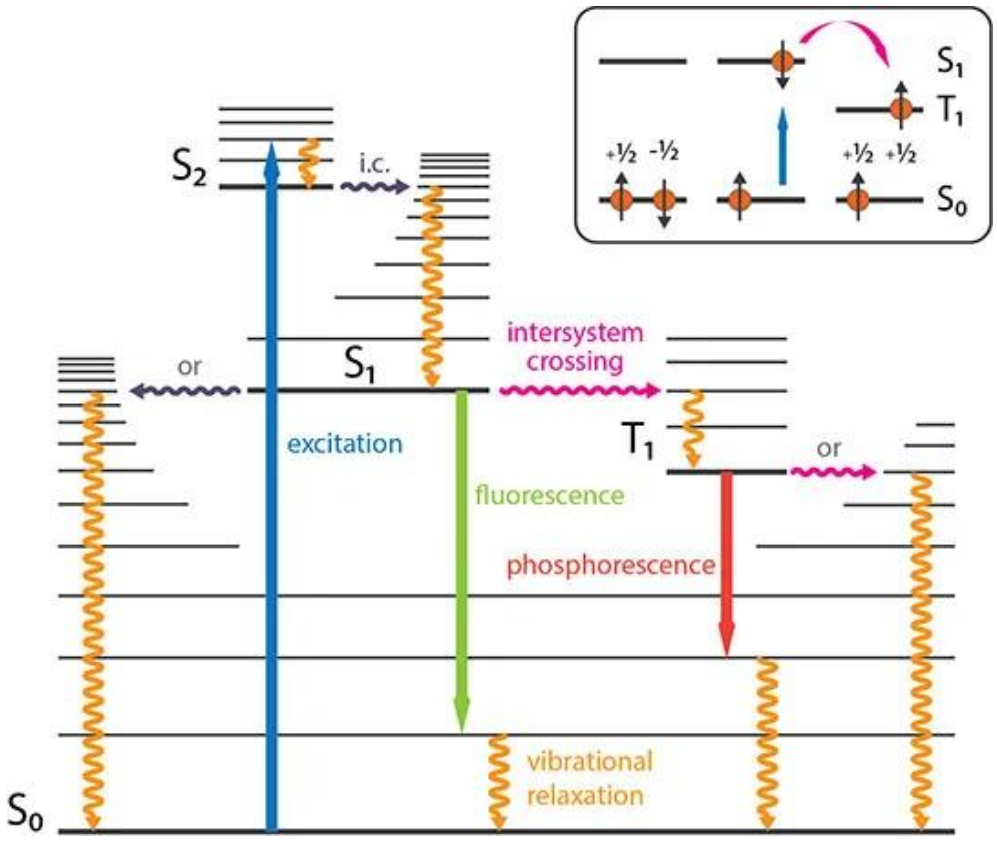

Figure 1.5: Jablonski Diagram (Phosphorescence and Fluorescence on materials)

1.6. APPLICATIONS AND USES

The property of phosphor to emit light in visible range even after the illumination has stopped due to bring a cold emitting materials i.e. there is no heat imparted to the material rather it has gone through some atomic- electronic level of transitions that has led it to be able to emit light, these properties are highly favourable and economical and enables users to use them for vast number of applications - from the TV screens to the CT scans, almost every industry and household uses these phosphor materials.

The very first type of application is w-LEDs (white LED), which uses Cerium-doped Yttrium Aluminium Garnet, a yellow phosphor, along with a blue chip. The blue light mixes with the yellow light; they are opposite each other on the colour wheel, and cancel each other out, giving the human eye what appears to be white light.

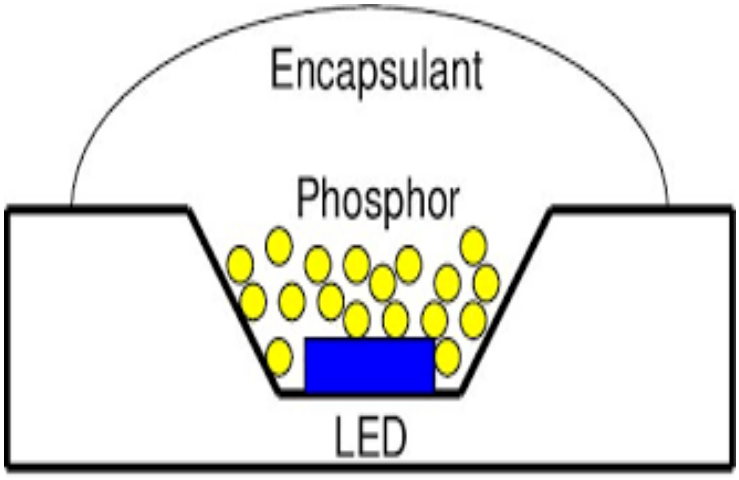

Figure 1.6: w- LED (White-LED)

Fluorescent lamps are another type of light emission source where the insides of a tube are coated with phosphor material, and they contain low-pressure mercury vapour. As the electricity is passed through this tube, it produces short-wavelength, high-energy UV radiation that is absorbed by the phosphor material to produce visible white light, due to fluorescence.

Full spectrum lighting, another way of getting sunlight (virtual one), is to produce a full spectrum of lights, red, yellow, green, etc, to combine and form what will act like virtual sunlight. The phosphors are used with blue LEDs to produce these, and their applications range from agriculture and horticulture to reptile or bird enclosures, museums, and therapy boppy boxes for Seasonal Affective Disorder (SAD) Treatment, as well as households and workplaces.

Figure 1.7: Agricultural Application of Phosphor using Full-Spectrum Lighting

Coming to the medical applications, the first and vital application is Computed Tomography (CT) Scanners. When the patient is exposed to X-rays, the transmitted X-rays are allowed to fall on a scintillator, which

amplifies the weak, attenuated signals and produces an electrical pulse. Now the pulse is allowed to fall on a photo detector, which again converts the rays into the visible range, allowing the computers to construct the patient's X-ray image.

Figure 1.8: CT scan

Positron Emission Tomography (PET) Scanners, as the radioactive decay must result in an electron and a positron pair, which get annihilated almost immediately to release gamma rays travelling in opposite directions with energy 511 keV. This concept is used, and the patients are usually injected with the radioactive material. The emitted gamma ray is allowed to fall on LSO OR LYSO scintillator crystals in the ring detector, which will tend to absorb the emitted rays almost simultaneously. The computers are then able to trace the exact location of the reaction and create a map of the annihilation event upon detection of the point where these rays hit.

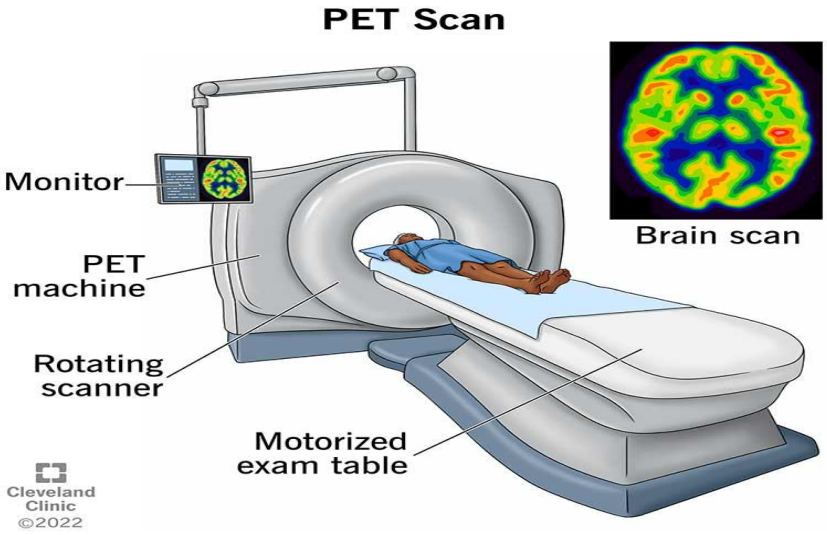

Figure 1.9: PET scan

Scintillators use these phosphor materials to produce images for scientific applications. The high-energy X-ray or Gamma rays are allowed to fall on a transparent crystal (like thallium-doped sodium iodide, NaI(Tl), or bismuth germane (BGO) which is very dense due to its high atomic number. They are absorbed, and the electrons are transferred between dynodes to produce a cascade of electrons. Now, these electrons are absorbed by an impure activator, which excites them and causes them to release low-energy visible photons as they return to their ground states.

CHAPTER – 2

CHARACTERIZATION TECHNIQUES

2.1. X-RAY DIFFRACTION PATTERN

One of the most well-known characterisation techniques that helps us to find the unique "fingerprint" of a crystal lattice. It is the most vital and primary type of characterisation that helps to guide the synthesis of the material. It can provide information about the crystal planes, how they deflect the X-rays, at what angles and the intensities of the deflected X-rays from these crystal planes.

6 Firstly, a monochromatic X-ray beam is directed onto the sample, where the wavelength of the X-rays is comparable to the interatomic spacing in the crystal lattice. Thus, when it hits the sample surface, it interacts with the atoms of the crystal lattice, which are arranged in regular patterns, and is deflected. Now, these rays that have bounced back will interact with each other, producing constructive and destructive interference patterns. The constructive interference is only shown when Bragg's law is satisfied, [5–7]:

$$n\lambda = 2d\sin(\theta) \tag{1}$$

Once we have the XRD data, we can compare it with the standard JCPDS peaks and check if we are going in the right direction, as in whether our material is synthesized correctly or not.

The Bragg's law is the key to relate the wavelength of the applied X-rays to the interplanar distance between them and the 'theta' angle of the diffraction. It says that when a material has an interplanar spacing of 'd in between its planes and an x-ray of the wavelength that has a similar or is comparable to the interplanar distance strikes the sample material, it will get diffracted and at only certain diffracted angles 'theta', it will give constructive interference and hence the diffraction or intensity peaks.

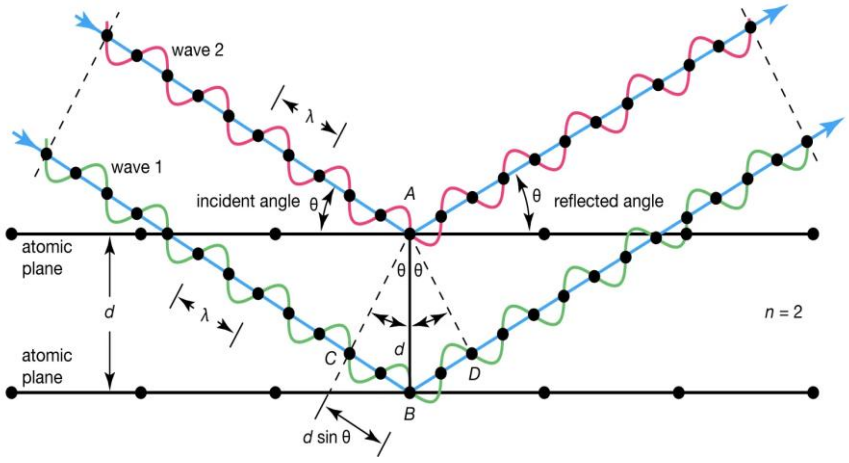

Figure 2.1: Bragg's Law Diagram

Since the sample has randomly arranged crystals and diffraction occurs from all planes of a particular crystal, we can say that similar planes contribute to a single diffraction peak. These planes are denoted by Miller indices (hkl) or reciprocal lattice points.

2.2. SCANNING ELECTRON MICROSCOPY (SEM)

Scanning electron microscopy is a type of microscopy that, just like any other microscopy, provides the user with a magnified image of the sample; however, the difference lies in the use of an electron beam that is highly focused, as compared to regular optical microscopes that use visible light that is present everywhere. An electron gun, whether a thermal emission one or a field emission one, is used that produces a highly focused beam of electrons that is focused directly onto the sample surface via condenser lenses and objective lenses. An interesting thing about the SEM apparatus is that it is performed in vacuum chambers to avoid collisions between the electron beam and dust and other gases in the air. Now, since the beams used are highly focused and energetic, the tiny electrons can be accelerated to high velocities, imparting high kinetic energy and greater ability to penetrate the sample surface.

The SEM data is capable of telling us about the surface morphology and the topography of the sample. This only happens due to the fact that electron beams interact with the surface, and as they are deeply penetrating, they can penetrate to layers deeper than that surface, thus interacting with a small volume around the electron beam spot. As they keep going deeper, they produce different types of rays and electrons that are detected by their specific detectors. The interacting beam produces secondary electrons, followed by the emission of back-scattered electrons that are coming from beneath the sample surface. Then, deeper lies the emission of X-rays and bremsstrahlung rays. Last but not least is the emission of cathodoluminescence rays. The auger electrons are also produced at the electron spot. The resolution is the best from the SE and BSE electrons only [8,9].

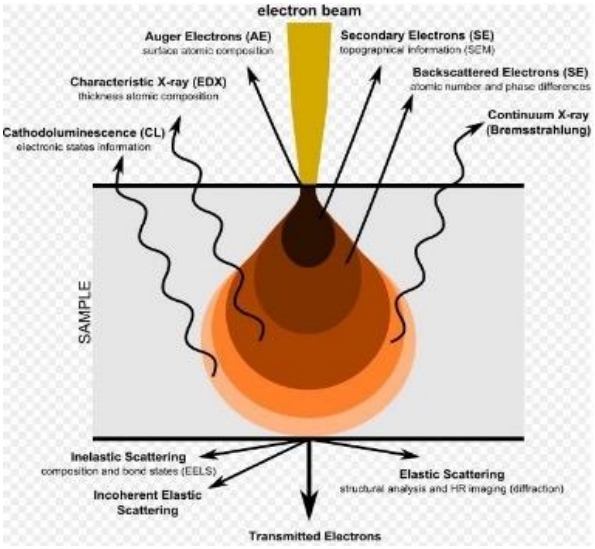

(a) Working Principle

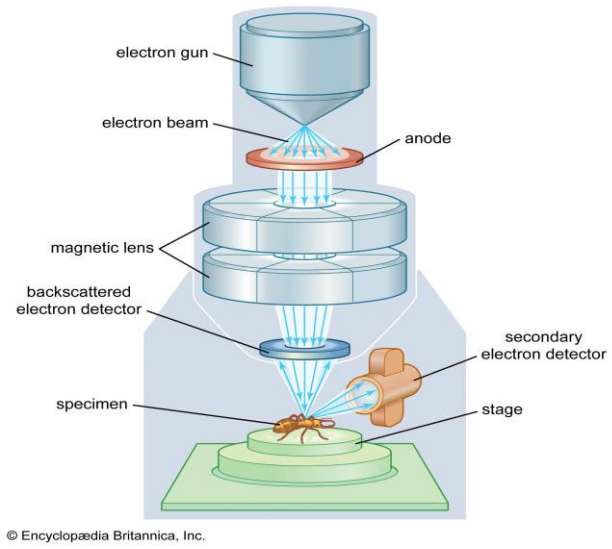

(b) Schematic Diagram

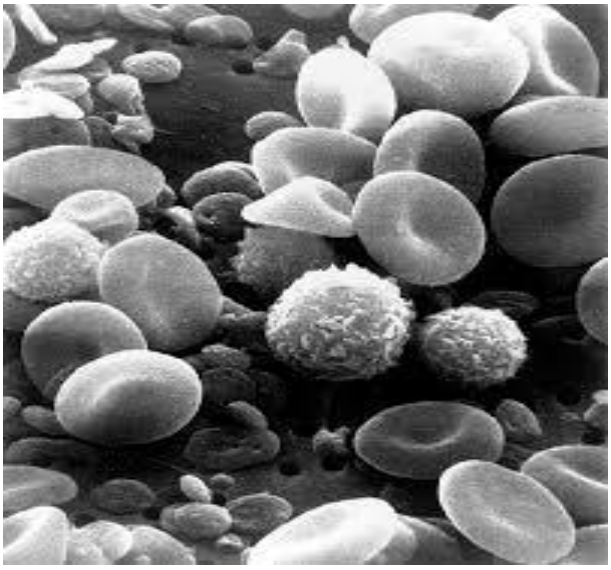

(c) Image of Blood cells using SEM
Figure 2.2: SEM characteristics and Images

SEM can be done for almost all types of solid or dried vacuum-compatible sample materials, whether it is conductive or non-conductive or a biological sample, such as residue of a gunshot, it barely makes a difference, as SEM is capable of finding the topographical and morphological structure of the surface of almost all samples, making it widely used. There can be limitations due to the accumulation of electrons on non-conductive surfaces. In such cases, the materials are coated with sputter-coating methods using gold or platinum to avoid this. Any type of material, bulk, thin film, powders, or nanomaterials are compatible with SEM.

2.3. UV- VIS- SPECTROSCOPY

Ultraviolet spectroscopy is a non-destructive, non-contact type of analytical technique that enables users to study the absorbance or transmittance of a sample. It is both a qualitative and a quantitative analytical technique.

Due to the presence of a chromophore, most materials are capable of absorbing Em waves of the UV-VIS range. The absorbance of such EM waves is governed by the Beer-Lambert law, which simply relates the path length, molar absorptivity and concentration to the absorbance of the material as a whole.

The Path length (unit in cm) is also referred to as the distance the light or EM wave has to travel before it can come out of the sample. It's also taken to be equal to the cuvette's width. Molar Absorptivity is rather a constant specific to the particular compound at a particular wavelength. It has units of M^{-1} cm^{-1}; it is also known as the material's extinction coefficient. Concentration (units M or mol/ L) is the concentration of the absorbing material that is present in the sample.

Beer-Lambert law relates these quantities and shows that they have linear dependence with the absorbance of material, as absorption is proportional to path length, as well as to molar absorptivity and then also to concentration, which implies that absorbance of material is proportional to all of these together as well. That's why the absorbance shows linear dependence on these quantities.

Instrumentation is quite simple; the apparatus requires a UV-VIS light source to provide the incident waves that will be directed to the sample by a wavelength selector-monochromator. As the light falls on the sample, the absorbance (or transmittance) will occur. Note that the apparatus is also equipped with a sample holder that holds the sample cuvette. As the light waves are absorbed (or transmitted), on the other side, a detector is waiting for the outgoing light to note its intensity.

So, if the wavelength of the applied wave is known to us and the detector tells us about the intensity of the outgoing waves, then the plot of these two will give us the required absorbance plot.

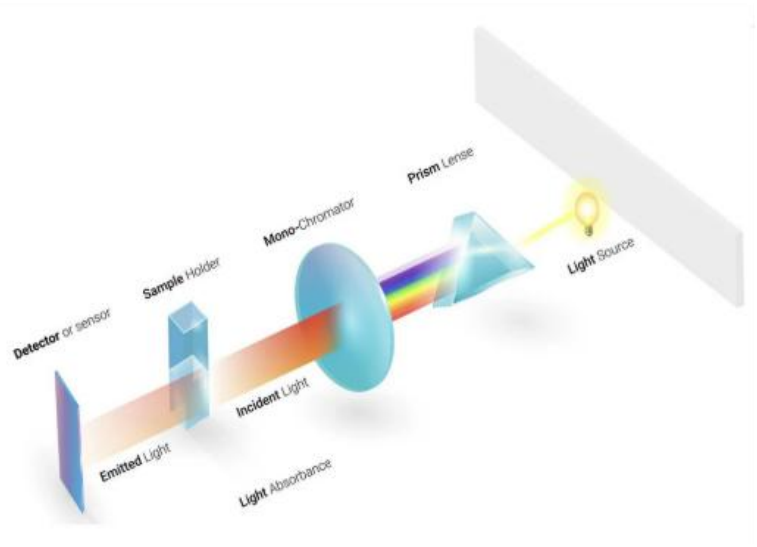

Figure 2.3: UV- VIS Spectrometer Working Principle

2.4. PHOTO LUMINESCENCE SPECTROSCOPY

Photo luminescence spectroscopy is the tool to study the emission and excitation spectra of a sample. It is non-destructive and non-contact in nature, enabling it to characterise nano materials, fluorophores, semiconductors, etc. It works on the simple phenomenon of electron–hole pair production and then annihilation.

Instrumentation is quite simple. First of all, there is a lamp that will act as the source of the EM waves. A xenon-arc lamp is used in the case of UV-VIS-NIR region waves. In other cases, the deuterium arc lamp is required when the UV radiation is needed. Secondly, lies the wavelength selector, a monochromator that allows users to pass a particular wavelength of the incident wave through onto the sample. There lies our sample holder containing the sample (at a 90-degree angle) as the radiation is incident on it; the excitation of electrons (electron–hole pair production) occurs. Thus, this incident

radiation is also referred to as the excitation wavelength. Once excited, the electron tends to lose its energy via a nonradiative process and becomes trapped in the sample's defects, also called trap states. From the trap, the electron will come back down and combine with the hole(annihilation). The energy difference of the two states is released as photons. The released photon then passes through another monochromator to allow only selected wavelengths of them to fall on the detector, and their intensity is noted.

The fluor spectrometers are equipped with different types of monochromators to fix one of the wavelengths, whether emission or excitation wavelengths, so that the intensity and the wavelength of the outgoing wavelength are noted carefully. When the exciting wavelength is fixed by the excitation monochromator, the outgoing waves reveal the different emission intensities and wavelengths, providing the emission spectrum.

Similarly, when the emission monochromator is fixed at a particular wavelength, only a single wavelength emitted by the sample is allowed to pass through. The sample is irradiated with different wavelengths of the incident beam so that the material is excited by different wavelengths coming from the lamp. Thus, by noting the wavelength that is exciting the sample and its intensity, the value is obtained.

This emission spectrum can further be used to find out the CIE plot, or the chromaticity plot, which is a 2D image that can describe the chromaticity or the colour of the emitted wave.

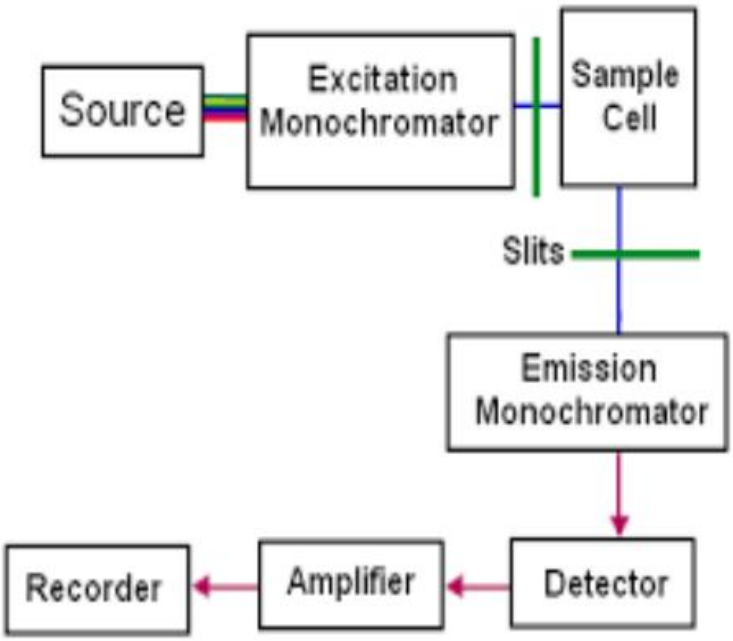

Figure 2.4: PL- Photo spectrometer working principle

CHAPTER - 3

SAMPLE PREPARATION

3.1 SOLID-STATE REACTION METHOD

The precursors $BaCO_3$, $SrCO_3$, Nb_2O_5, and Eu_2O_3 were used to synthesise $Ba_3SrNb_2O_9$: xEu^{3+} phosphors with different Eu^{3+} concentrations (x = 1.0, 3.0, 5.0, 7.0, 9.0 mol%) using the solid-state method. The chemical precursors were employed in stoichiometric proportions and mixed thoroughly. To achieve homogeneity, the mixture was ground in an agate mortar using a pestle. The resulting mix was then transferred to an alumina crucible and calcined in an electric furnace at 1373K for 5 hours, with a controlled heating rate of 5 °C/min under room temperature. After heating, the prepared powdered samples were left inside the furnace to get cooled to room temperature under the same atmospheric conditions. This process ensured complete oxidation of the constituent ions and promoted the formation of a stable layered perovskite structure. Eventually, the procured material was ground into an ultra-fine powder for further characterisations [4,10,11].

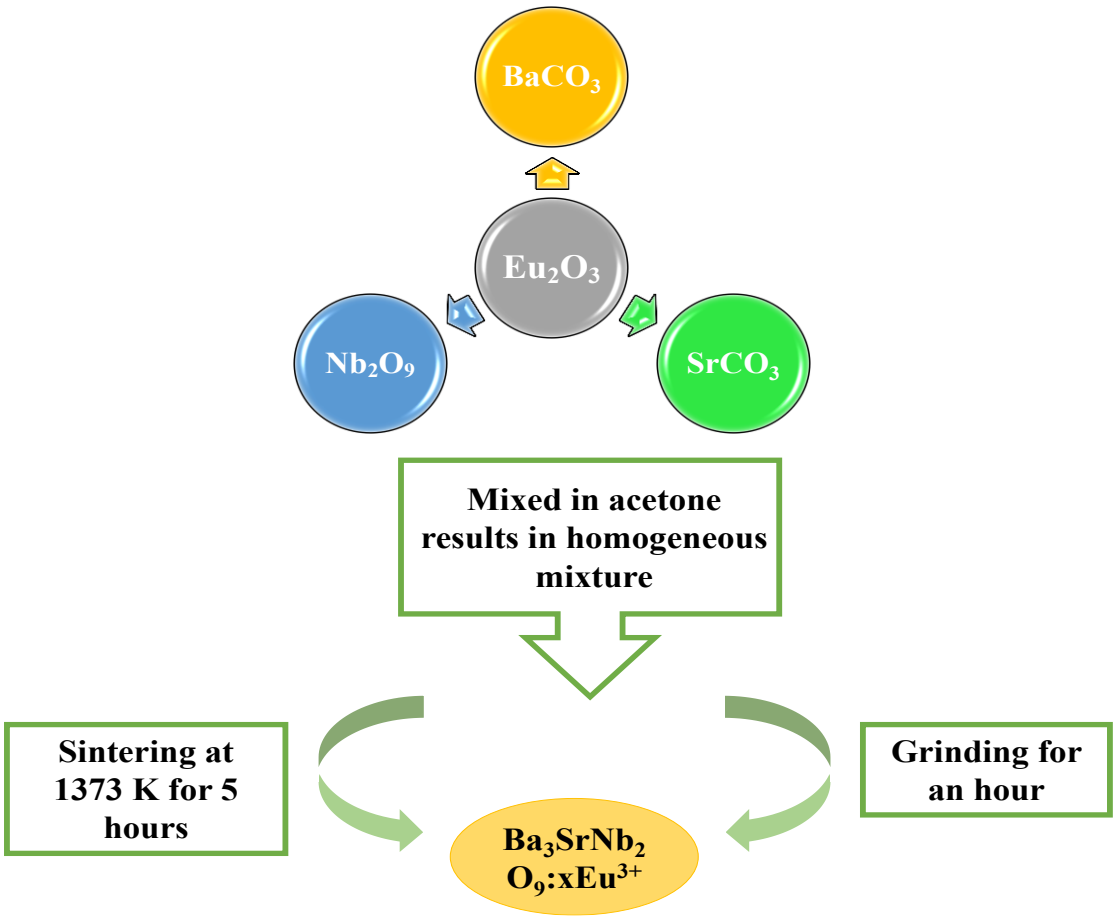

Figure 3.1: The process of synthesis of BaSN phosphor with Eu^{3+} activator ions

CHAPTER - 4

RESULTS AND ANALYSIS

4.1. X-RAY DIFFRACTION ANALYSIS

X-ray diffraction (XRD) patterns of undoped BaSN and doped BaSN: Eu^{3+} phosphors are depicted in Fig. 4 .1 (a). The diffraction peaks of all the synthesized powdered samples show good match with the standard JCPDS-04-016-9398 data, verifying successful formation of the crystalline BaSN phase and absence of impurity peaks.

The observed XRD data for the synthesized samples have a hexagonal crystal system along with a P63/m space group and 176 space group number. The lattice parameters are a = 6.070 Å, b = 6.070 Å, c = 15.376 Å, $\alpha = \beta = 90^{\circ}$, $\gamma = 120^{\circ}$, and volume of the unit cell is 490.63×10^6 pm^3. The sharp diffraction peaks reveal high crystalline nature of the prepared phosphor. After incorporation of Eu^{3+} ions, the diffraction peaks of the prepared powdered samples showed good agreement with the JCPDS data, validating Eu^{3+} ions are successfully substituted into the lattice without causing major structural distortion or secondary phase formation.

The crystallite size was calculated using the Debye-Scherrer formula as expressed below [12,13], by employing the major peaks of the X-Ray Diffraction pattern:

$$D = \frac{K\lambda}{\beta \cos\theta} \quad (2)$$

Here, λ is the X-ray wavelength (1.54 nm), θ is the diffraction angle, β is the full width at half maxima (FWHM), K is a constant with value 0.94, and D denotes the crystallite size. The average crystallite size was determined to be 42 nm for the undoped BaSN phosphor.

The Williamson–Hall (W–H) plots for undoped and Eu^{3+}-doped BaSN phosphors are shown in Fig. 4 .1 (b). The W–H relation is expressed as[14,15]:

$$\beta \cos(\theta) = \frac{K\lambda}{D} + 4\,\epsilon \sin(\theta) \quad (3)$$

where β is the full width at half maximum (FWHM), D denotes the crystallite size, ϵ represents the lattice strain, k is the shape factor, and λ denotes the X-ray wavelength. The crystallite size is calculated from the intercept of the linearly fitted line, while the slope gives the lattice strain value.

When compared to the undoped BaSN sample, the Eu^{3+}-doped BaSN phosphor shows a slight variation in

slope, suggesting modification of lattice strain because of the incorporation of Eu^{3+} ions into the host matrix. The relatively small values of strain validate that the crystal lattice possesses good structural stability after the introduction of the activator ions.

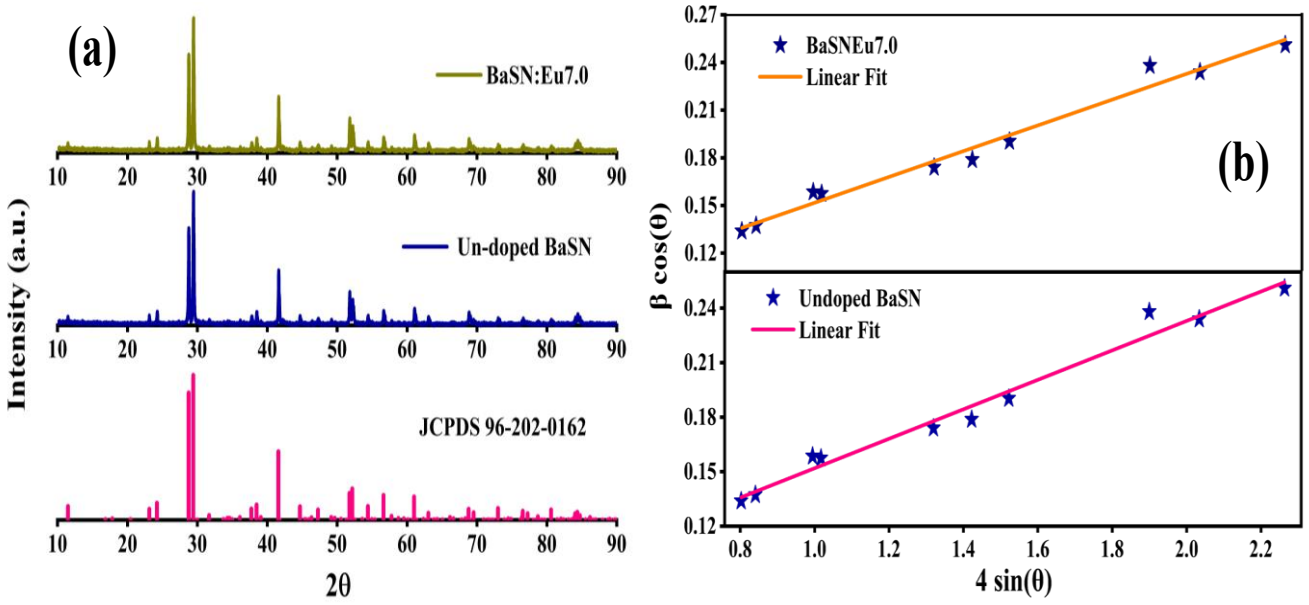

Figure 4.1: (a) XRD plots of undoped and doped BaSN phosphor with 7.0 mol% concentration of Eu^{3+} ions, accompanied by the standard JCPDS data **(b)** W-H Plot

4.2. SCANNING ELECTRON MICROSCOPY - MORPHOLOGICAL STUDIE

SEM images for the undoped and doped BaSN with 7.0 mol% concentration of Eu^{3+}, and the particle size distribution histogram is shown in Figure 4.2. The particles are typically in the range of 1-2 μm and appear to be agglomerated, which could be a result of manual grinding and high-temperature sintering during preparation [16,17]. Since smaller particles have a higher surface-to-volume ratio than larger ones, they are more likely to stick together and form large clusters due to their greater surface energy. To enhance the stability and reduce surface energy, phosphor particles within the micrometer size range are considered more suitable for use in WLED. Fig. 4.3 displays the EDX images of the undoped BaSN sample, confirming the presence of all the intended precursor elements within the lattice.

EDX plots the energy produced by X-rays vs. the count of photons, provides us with a histogram of data, which is essential for understanding and knowing the chemical composition of the sample. Fig 4.3 illustrates the distribution of particle size as a histogram, indicates that majority of the particles lie in this range, thereby demonstrating its suitability for solid-state lighting applications.

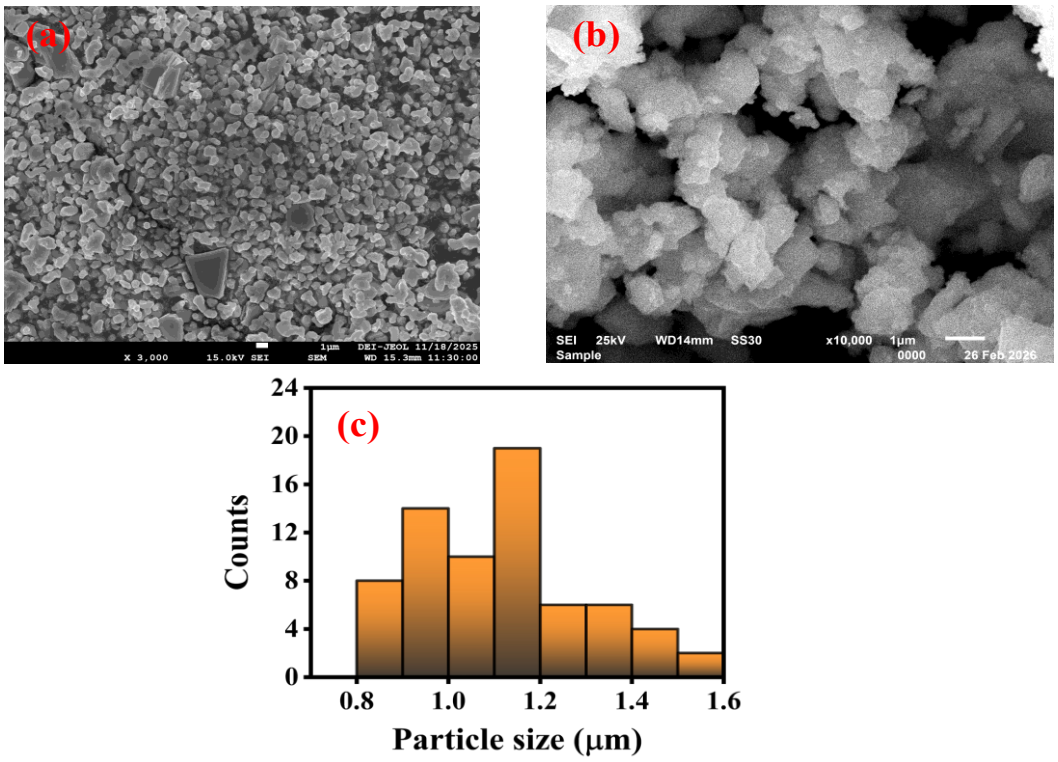

Figure 4.2: (a) SEM image for undoped BaSN, (b) For doped BaSN phosphor with 7.0 mol% concentration of Eu^{3+}, **(c)** Particle size distribution histogram obtained from SEM analysis.

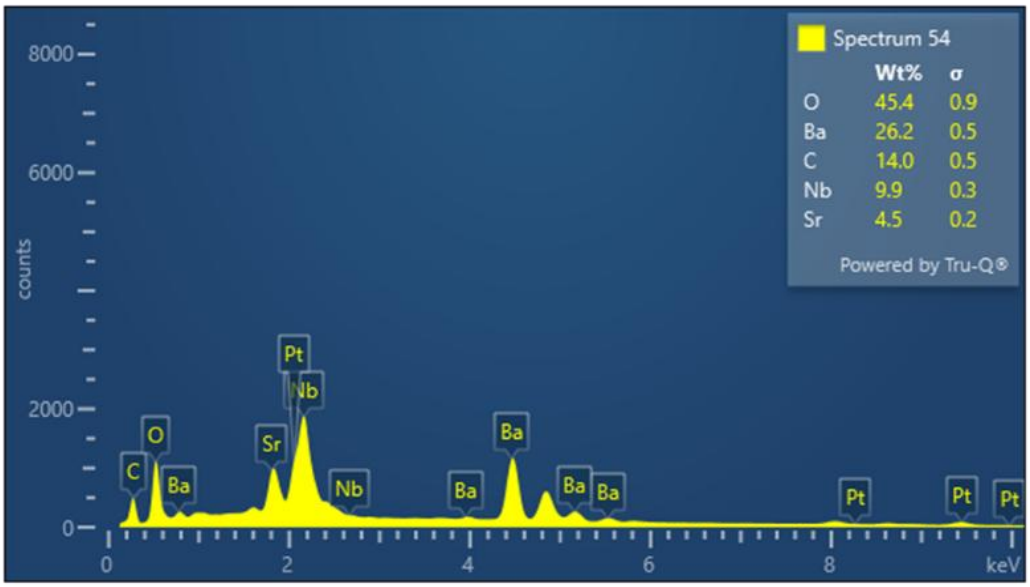

Figure 4.3: EDX image of the undoped BaSN phosphor

4.3 FT-IR ANALYSIS

The Fourier Transform Infrared (FT-IR) spectra of undoped and 7 mol% doped BaSN phosphor sample were recorded in the 400-4000 cm-1 range, and were used to analyse the bonding characteristics and structural framework, as illustrated in Fig. 4 .4. A broad band around ~3200-3400 cm^{-1} combined with O–H stretching vibrations, indicates the presence of moisture absorbed, while a weak band is ascribed to H-

O-H bending vibrations near ~1600 cm^{-1}. The region (400-1000 cm^{-1}) provides key structural information, where the strong band nearly ~800-850 cm^{-1} is assigned to Nb-O stretching vibrations of NbO_6 octahedra, verifying the formation of the niobate network. The band near ~600-700 cm^{-1} is combined with Nb-O-Nb bridging vibrations, whereas the absorption below ~600 cm^{-1} is obtained from Ba-O/Sr-O metal–oxygen vibrations.

The addition of Eu^{3+} ions indicates no appreciable change in the overall FTIR profile, suggesting that the host lattice is structurally stable. However, the slight shifts and variations in intensity, specifically near ~885 cm^{-1}, demonstrate distortion in local structure caused by the substitution of Sr^{2+} (1.44 Å) by the smaller Eu^{3+} ions (~1.23 Å). This mismatch in ionic radius induces localised strain and modifies the Nb-O bond environment within the NbO_6 octahedra. In spite of these changes, the absence of new bands validates successful doping of Eu^{3+} ions within the host lattice, without the formation of secondary phases; this was further supported by XRD results.

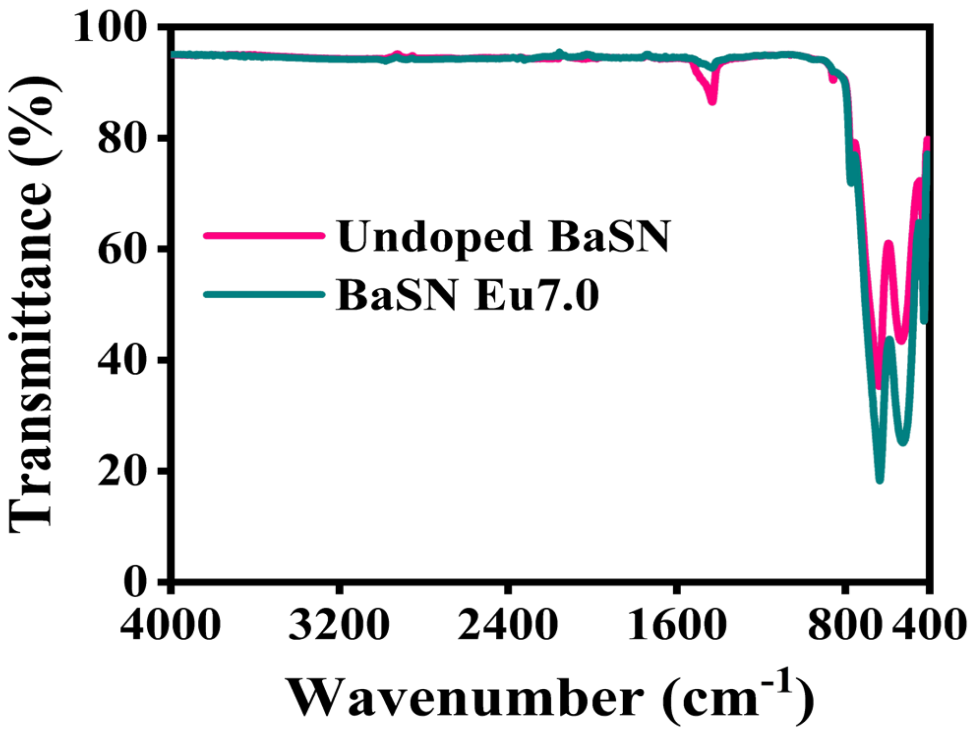

Figure 4.4: Fourier-transform infrared spectra for undoped BaSN and BaSN:Eu7.0 phosphors.

4.4 THERMOGRAVIMETRIC ANALYSIS (TGA)

To evaluate the thermal stability and decomposition behaviour of the synthesised undoped BaSN phosphor with temperature, the Thermogravimetric analysis was performed. As shown in Fig. 4.5, the TGA curve was observed over the temperature range of approximately 200-1100°C, indicating substantial overall weight loss.

From the graph, it is observed that the sample exhibits good thermal stability over a broad temperature

range. At first, the sample exhibits almost no significant weight loss between 200°C and around 650-700°C, demonstrating the absence of moisture and volatile impurities. A decrease in weight percentage was observed beyond 700°C, followed by a more prominent weight reduction at temperatures beyond this. This behaviour implies the onset of thermal decomposition and lattice distortion in the host lattice. The significant weight loss occurs in the region between nearly 750°C and 1000°C, probably due to the decomposition of residual precursor compounds, the release of moisture, or the breakdown of unstable chemical bonds within the lattice.

The total observed weight loss is nearly 14.76%, as shown in the graph. Even after heating up to 1100°C, the sample retains nearly 85% of its original mass, demonstrating comparatively high thermal durability.

Initially, the lower mass variation, together with moderate overall weight loss, suggests that the synthesised sample possesses good thermal resistance and structural stability, suitable for optoelectronic applications such as white LEDs. The TGA results thus confirm that the prepared phosphor material exhibits good thermal stability with limited decomposition at higher temperatures.

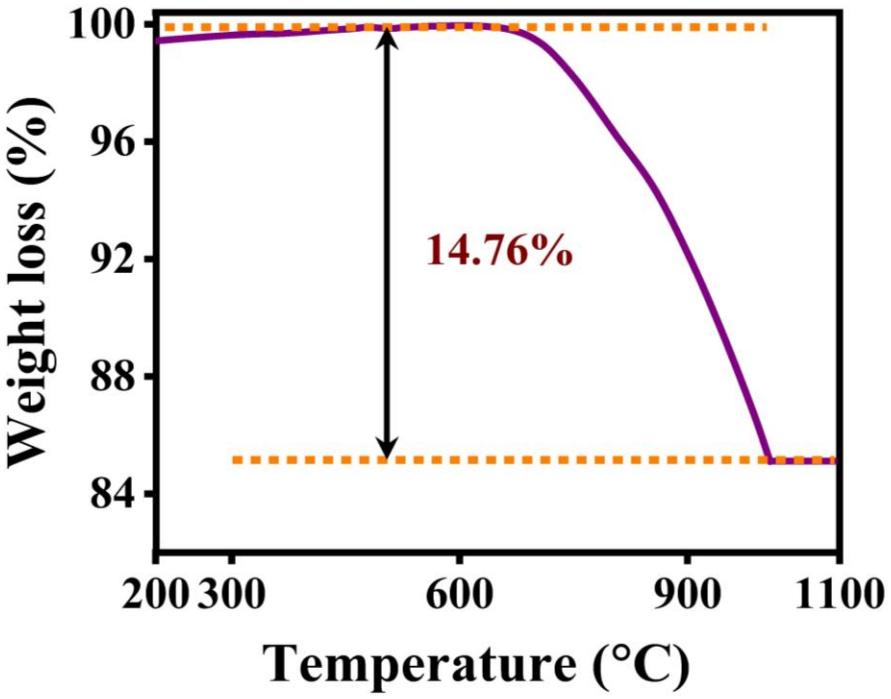

Figure 4.5: TGA analysis of un-doped BaSN sample.

4.5 DIFFUSE REFLECTANCE SPECTRA (DRS):

The diffuse reflectance spectra (DRS) of undoped and Eu^{3+}-doped BaSN phosphors observed in the of 200-800 nm wavelength range, as shown in the figure. The DRS study was conducted to evaluate the optical absorption behaviour and the electronic structure of the synthesised powdered phosphors.

From the spectra, an intense absorption band is observed in the ultraviolet region, centred around 240–280

nm, corresponding to charge-transfer transitions associated with the host lattice. A prominent reflectance peak is observed at 300-330 nm for all compositions, indicating a strong interaction between incident photons and the electronic states of the host lattice. Beyond this wavelength region, the reflectance gradually decreases and approaches stability in the visible region.

As the concentration of Eu^{3+} ions increase, the slight variations in the reflectance intensity are observed, indicates effective incorporation of Eu^{3+} ions into the host lattice. The reduced reflectance in certain wavelength regions for doped powdered samples suggests increased optical absorption due to the incorporation of Eu^{3+} ions. The wide absorption behavior in the UV region verifies absence of secondary irregularities in the spectra[18,19].

The calculation of the optical bandgap is crucial while considering the properties of an LED. DRS data observed for BaSN:xEu^{3+} (x=1.0 - 9.0 mol%, Δx = 2 mol%) phosphors over the wavelength range of 200-800 nm, as shown in Fig. 4 .6, were converted into a Kubelka-Munk absorption function, F(R) to evaluate the optical band-gap value, as expressed below[20,21]:

$$F(R) = \frac{(1-R)^2}{2R} = \frac{K}{S} \quad (4)$$

Here, K and S are the Absorption and scattering coefficient , respectively and R is the reflectance of samples. The Tauc equation shows the relationship between the absorption coefficient and the bandgap energy, Eg, as expressed below[11,22]:

$$\alpha(v) = \frac{B}{hv}\left(hv - E_g\right)^n \quad (5)$$

Here, hυ is the photon energy, , *n* represents the different types of electronic transitions, and its value is either 1/2 or 2 depending on the nature of the transition - direct or indirect transition, respectively. The above equations demonstrate that the F(R) is directly proportional to α, thus Tauc equation is illustrated as[22,23]:

$$F(R)\ h\nu = C\left(h\nu - E_g\right)^{n/2} \quad (6)$$

The Tauc plot is the graph plotted between hν and $[F(R)h\nu]^2$ to evaluate energy bandgap value of BaSN:xEu^{3+} phosphor. As we extrapolate the line in the linear region of the plot, we obtain the optical band gap Eg, as shown in the Fig 4.7. The band gaps of BaSN:xEu^{3+} (x=1.0, 3.0, 5.0, 7.0, 9.0 mol%) were obtained to be 4.51, 4.47, 4.34, 4.31, 4.29 and 4.27, respectively. The decreasing bandgap can be explained by the development of intermediate energy levels in the rare earth (RE) ions (Eu^{3+}). While increasing the concentration, the expansion caused by the presence of the activator ions in the unit cells of the host lattice results in the widening of the energy band gap and subsequently narrowing of the valence and conduction band [10,24].

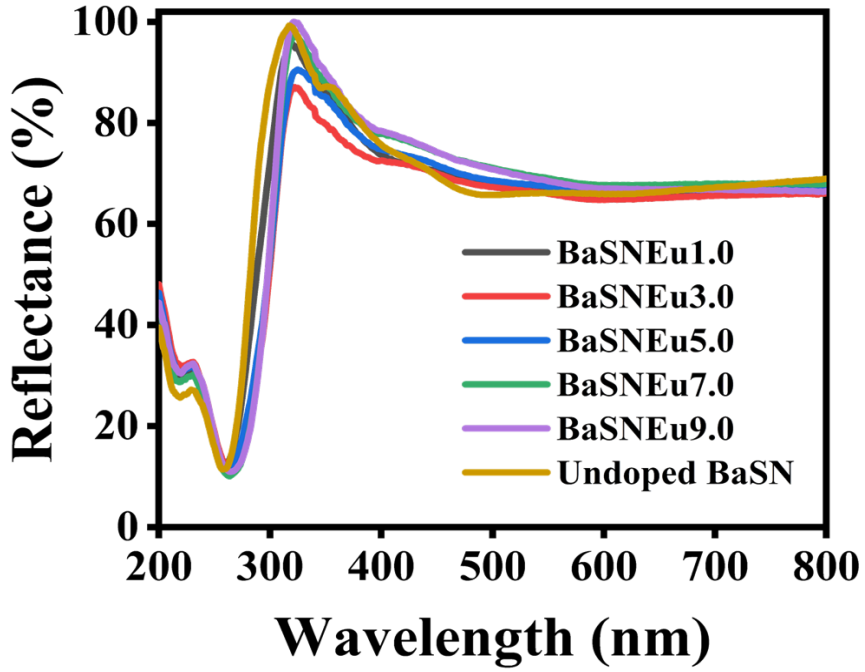

Figure 4.6: Diffuse Reflectance Spectra of undoped and doped BaSN with Eu^{3+} ions at varying mol% concentration.

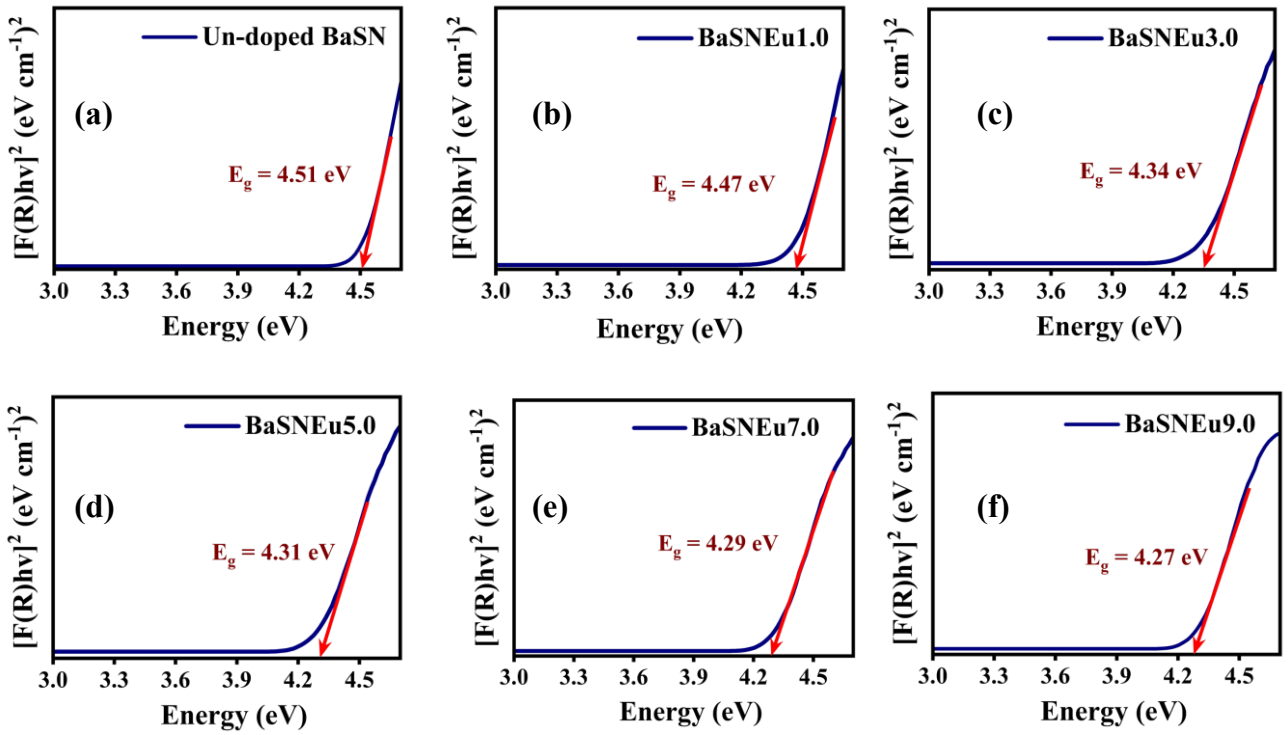

Figure 4.7: Tauc plots of BaSN:xEu^{3+} (x=1.0, 3.0, 5.0, 7.0, 9.0 mol%) for optical bandgap calculation.

Table 1. Calculated Band gap energy values for different mol % of Eu^{3+} ions in the BaSN phosphor

S.No.	Sample (mol %)	Band gap (eV)
1.	Undoped	4.51
2.	1	4.47
3.	3	4.34
4.	5	4.31
5.	7	4.29
6.	9	4.27

4.7 PHOTOLUMINESCENCE (PL) SPECTROSCOPY ANALYSIS:

To investigate the photoluminescent characteristics of phosphors, the excitation spectra of as-prepared Eu^{3+} doped BaSN phosphor were analyzed and depicted in Fig 4.8(a). The excitation spectra were recorded in the range of 350-500 nm wavelength. The excitation spectrum is comprised of f → f transitions of Eu^{3+} ions. There is a strong intense peak at 395 nm corresponding to $^{7}\mathbf{F_0} \rightarrow {}^{5}\mathbf{L_6}$. As the excitation band was observed at 395 nm wavelength corresponding to $^{7}\mathbf{F_0} \rightarrow {}^{5}\mathbf{L_6}$ transition with the highest intensity, the emission analysis was done by exciting all the as-prepared Eu^{3+} ions doped phosphor samples at 395 nm[4,10,25]. The Eu^{3+} ions doped BaSN phosphors were excited at 395 nm, systematic emissions at 592 nm were observed. The Photoluminescence emission spectra recorded at the 395 nm excitation have edged peaks at 580, 592, 612 and 660 nm, ascribed to the transitions from $^{5}D_0$ to $^{7}F_0$, $^{7}F_1$, $^{7}F_2$, and $^{7}F_3$ of Eu^{3+} ions respectively, as depicted in Fig 4.8(b)[26,27]. The $^{5}D_0 \rightarrow {}^{7}F_2$, electric dipole (ED) transition is very sensitive to the dopant surrounding environment therefore, hypersensitive to the inversion symmetry distortions while, the transition $^{5}D_0 \rightarrow {}^{7}F_1$, is a magnetic dipole (MD) transition contrary to the surrounding environment. Moreover, the emission spectra confirms that the ED transition, $^{5}D_0 \rightarrow {}^{7}F_2$ is dominated by the MD transition, $^{5}D_0 \rightarrow {}^{7}F_1$ [28]. The emission spectra intensity increases systematically with the increasing concentration of the Eu^{3+} ions and achieves highest value at 7.0 mol%, beyond this concentration a decrease in the emission intensity is triggered due to concentration quenching, illustrated in Fig. 4.8 (b). This quenching mechanism is caused by the dipole-dipole interactions between the Eu^{3+} ions and contracted interionic distance at higher dopant levels [29].

The Dexter's theory, which establishes a relation between photoluminescent intensities and doping concentration, is used to determine the type of multipolar interaction with the help of the equation, expressed below[7,30]:

$$\log\frac{I}{x} = A - \frac{s\log(x)}{3} \quad (7)$$

Here, A is a constant not dependent on dopant concentration and I is the emission intensity. The value of s which is either 6, 8, or 10 is used to specify the nature of interaction as either dipole-dipole, dipole-quadrupole, and quadrupole-quadrupole, respectively[31]. The slope of the fitted curve between log(1/x) and log(x) is equal to (s/3), shown in the Fig 4.9(a). The calculated value of the slope came out to be 1.72, when multiplied by 3, value comes out to be narrowly close to 6, indicating dipole-dipole interaction as the reason behind the concentration quenching among Eu^{3+} ions.

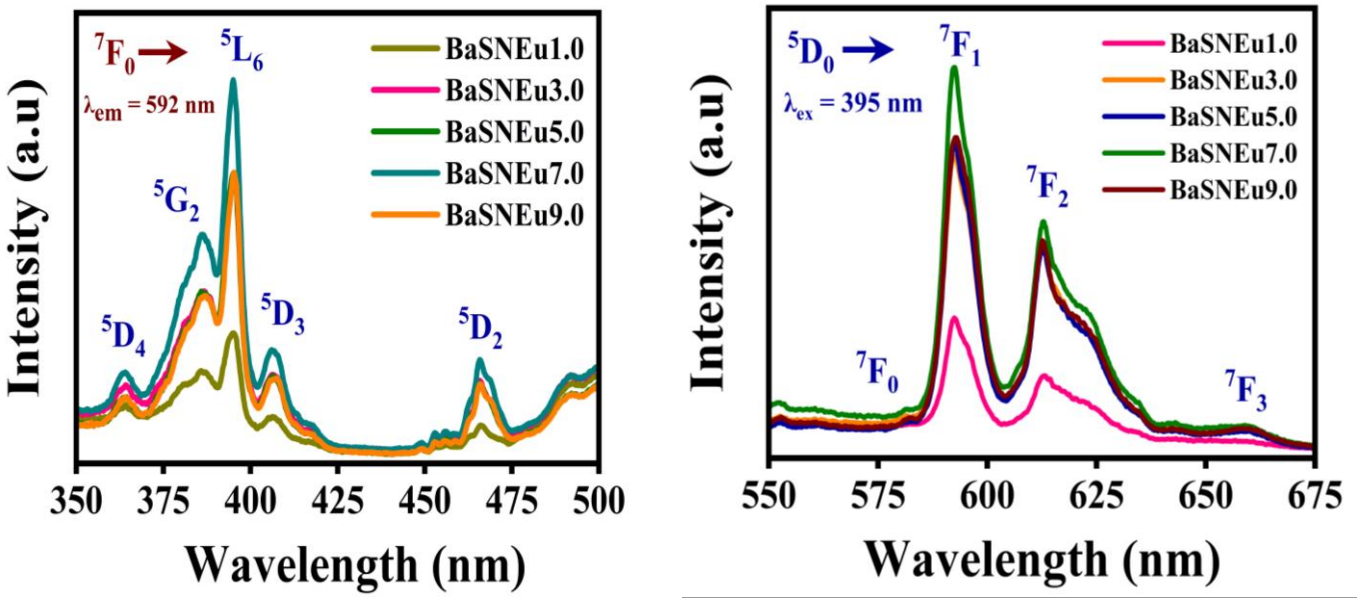

(a) **(b)**

Figure 4.8: (a) Excitation spectra, and **(b)** Emission spectra of BaSN phosphor with varying Eu^{3+} ions concentration

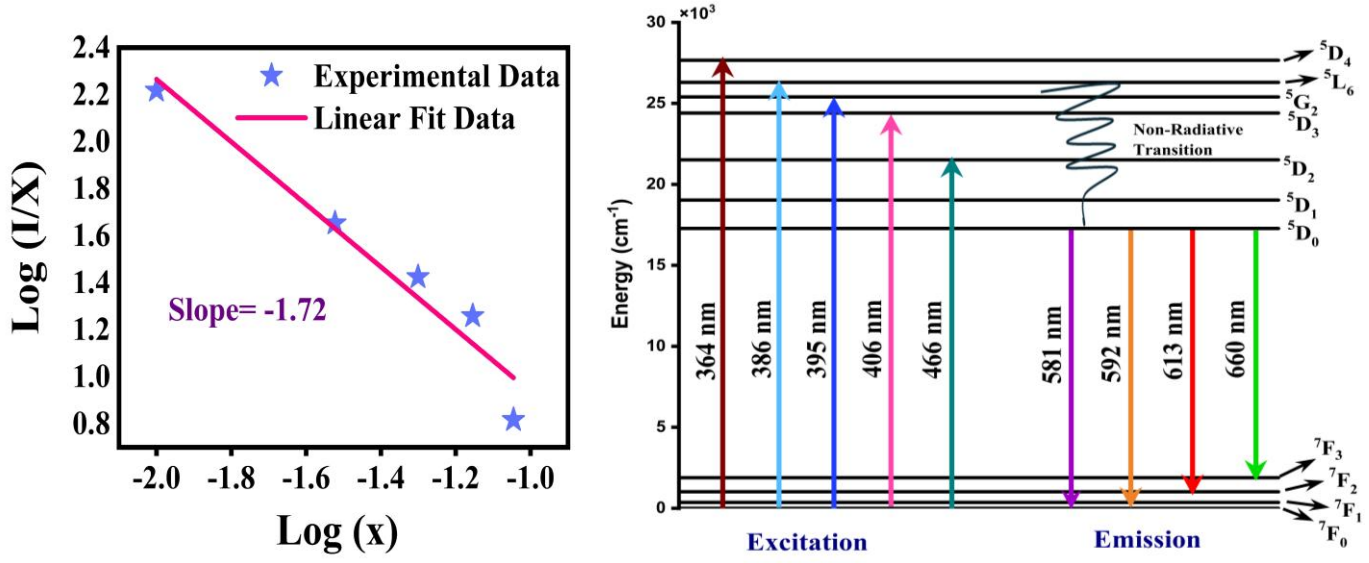

(a) **(b)**

Figure 4.9: (a) Plot of log(1/x) vs. log(x) **(b)** Energy levels and possible channels of Cross-relaxation for BaSN:xEu^{3+} phosphor

[24]

4.8 PL DECAY CURVE ANALYSIS:

The Photoluminescence decay curves of the synthesised BaSN:xEu3+ (x =1-9 mol%, Δx = 2 mol%) phosphors were recorded and depicted in Figure 4.10. The decay curves were recorded at excitation and emission wavelengths of 395 nm and 592 nm, respectively, at room temperature, to evaluate the luminescence properties and energy transfer mechanism of the powdered samples. The obtained decay plots were fitted with a biexponential decay function at all concentrations, indicating that the luminescent system contains more than one relaxation process. The decay curves follow the following equation[32]:

$$I_t = I_0 + A_1 \exp\left(-\frac{t}{\tau_1}\right) + A_2 \exp\left(-\frac{t}{\tau_2}\right) \quad (8)$$

Here, I_0 represents the initial intensity at time, t=0, and I represent the intensity at a time, t. A_1 and A_2 stand for the decay constants amplitude, and τ_1 & τ_2 represent the luminescent decay lifetimes. The average decay lifetime is calculated from the formula shown below [5,23]:

$$\tau_{avg} = \frac{A_1\tau_1^2 + A_2\tau_2^2}{A_1\tau_1 + A_2\tau_2} \quad (9)$$

From Fig 4.10, it was analysed that the intensity of decay curves was decreasing gradually with the increase in Eu^{3+} ions concentration in the prepared samples. The calculated decay time is in milliseconds range. The decay lifetime value decreases continuously with increasing concentration of activator ions from 1mol% to 9 mol%. This reduction in decay lifetime could be attributed to the non-radiative transfer of energy among the Eu^{3+}- Eu^{3+} ions at shorter interionic distances. With increasing concentration of the dopant ions, the possibility of cross-relaxation and multipolar interaction also increases, which results in a faster non-radiative decay process. The calculated radiative lifetime value was found to be 1.970 ms, indicating efficient luminescent behaviour of the prepared samples. Fig 4.10, illustrates the change in decay lifetime with variation in Eu^{3+} concentration.

Furthermore, to study the decreasing lifetime of the powdered samples with increasing Eu^{3+} ions concentration further investigations were done by using the Auzel's model, expressed below[33,34]:

$$\tau = \frac{\tau_0}{\left(1 + \frac{c}{c_0 e^{-\frac{N}{3}}}\right)} \quad (10)$$

Here, N represents the number of phonons produced during the relaxation process, c stands for the concentration of Eu^{3+} ions, τ_0 denotes the intrinsic radiative lifetime, while τ is the estimated lifetime. It has been observed that to fit well in the Auzel's model as shown in the Fig 4.10, the value of intrinsic lifetime τ_0, is calculated to be 1.970 ms.

To further evaluate the energy transfer mechanism, the decay curves are again fitted by the Inokuti–

Hirayama (I–H) model, as illustrated in Fig.4.11. The fitting was done by assuming s = 6, as it corresponds to the dipole-dipole (d-d) interaction among the Eu^{3+} ions. It is confirmed from the fitted curves that the dipole – dipole interaction is the dominant mechanism responsible for the energy transfer in the BaSN:Eu^{3+} phosphors. The I–H model is represented as[35]:

$$I_t = I_0 \times \exp\left(\left(-\frac{t}{t_0}\right) - Q \times \left(\frac{t}{t_0}\right)^{\frac{3}{s}}\right) \quad (11)$$

Here, Q stands for the energy transfer mechanism, while the time, t_0 is the donor lifetime. The parameter "s" demonstrates the type of the interaction among the dopant ions in a host lattice. The particular value of s = 6, s = 8 and s = 10 correspond to the dipole-dipole (d-d), dipole-quadrupole (d-q) and quadrupole–quadrupole (q-q) interactions, respectively. The particular value of s = 6 here, showed that here the main energy transfer mechanism among the Eu^{3+} ions within the BaSN phosphors is the dipole-dipole (d-d) interaction, also matches with the Dexter's theory of energy migration.

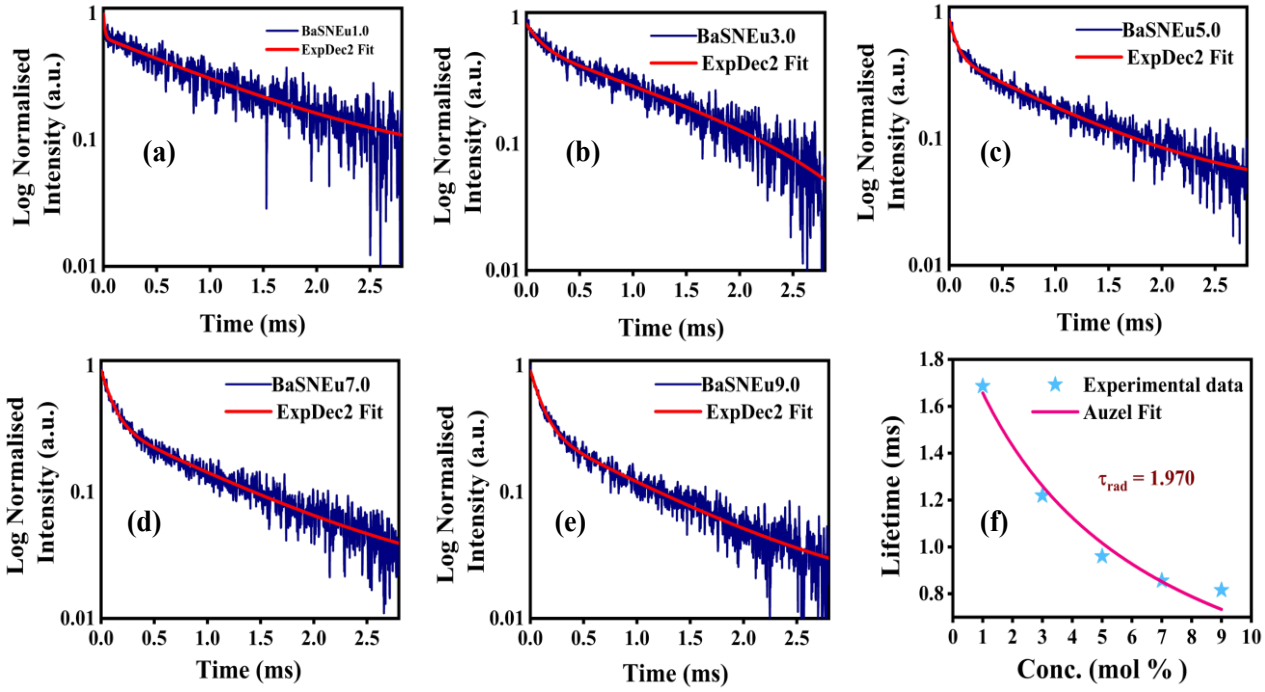

Figure 4.10: PL decay plots for Eu^{3+} doped BaSN phosphor with Eu^{3+} concentrations (x=1.0, 3.0, 5.0, 7.0, 9.0 mol%)) at λ_{ex}= 395 nm

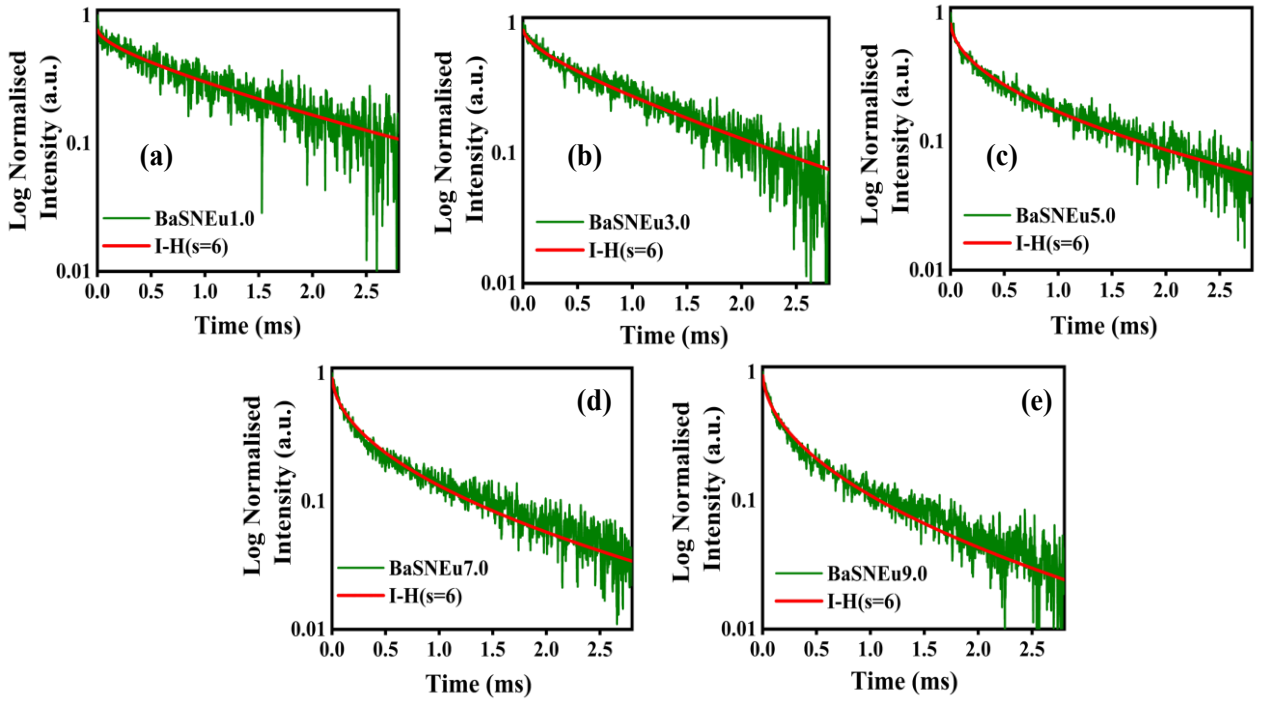

Figure 4.11: The Fitted curves by I-H model for BaSN doped phosphors with Eu^{3+} concentrations (x=1.0, 3.0, 5.0, 7.0, 9.0 mol%) doped

Table 2. The Lifetime of the BaSN:xEu^{3+} phosphor for x=1.0 - 9.0 mol%, Δx = 2 mol%

Concentration of Eu^{3+} ions	Lifetime (τ)
1.0	1.162
3.0	1.698
5.0	0.884
7.0	0.907
9.0	0.815

4.8 COLORIMETRY ANALYSIS:

Colorimetry, specifically using the CIE coordinates, is one of the methods used to evaluate the color output of phosphor materials in a standardized way. When a phosphor is excited by a near-UV or visible light—it emits light of a certain color. To understand and quantify this color, researchers measure the emission spectrum of the material and further use this to calculate the CIE (Commission Internationale de l'Éclairage) chromaticity coordinates[36].

These coordinates are represented on a Two-dimensional chromaticity diagram as (x, y), which help human eye to pinpoint the exact color. The Chromaticity diagram includes all visible colors thus, represents the entire visible spectrum, and the location of the coordinates gives a clear visual indication of the material's

emitted color. For instance, coordinates near the blue region indicates blue emission, while points closer to the center suggest white or near-white light. To evaluate the chromatic behaviour of the BaSN:xEu^{3+} ions (x=1.0 - 9.0 mol%, Δx = 2 mol%) phosphor, we utilized the CIE chromaticity coordinates from PL emission spectra under 395 nm excitation wavelength, as illustrated in the Fig 4.12.

The color purity (CP) of the prepared phosphor samples is a crucial factor for the evaluation of the colorimetric behaviour and was employed to investigate the color stability of the prepared samples. The color purity formula is illustrated below[30]:

$$CP = \frac{\sqrt{(x-x_{ee})^2+(y-y_{ee})^2}}{\sqrt{(x_d-x_{ee})^2+(y_d-y_{ee})^2}} \quad (12)$$

Here (x_{ee} ,y_{ee}) represent equal energy coordinates, (x,y) show the color coordinates of BaSN phosphor, while (x_d, y_d) are the dominant wavelength coordinates.

The color purity of the as-synthesized phosphor under 395 nm excitation wavelength was calculated to be 89.51%. The high color purity of BaSN phosphor demonstrates its excellent emission characteristics and use in various solid-state lightning applications[37,38]. Additionally, the values of the correlated color temperature (CCT) for the Eu^{3+}-doped powdered lie in range of 2873 and 4348 K. This relatively low CCT range suggests that the phosphor is well-suited as a warm-red light emitter, making it a promising component for white LED applications[7,39,40].

Table 3. displays the evaluated CIE coordinates (x,y) accompanied by the color correlated temperature (CCT) values for the BaSN:xEu^{3+} phosphors with different Eu^{3+} ion concentrations. The obtained CIE coordinates lie in the Red-Orange region, as illustrated in the Fig 4.12, implying suitability of the synthesized phosphor is solid-state lighting devices and display panels.

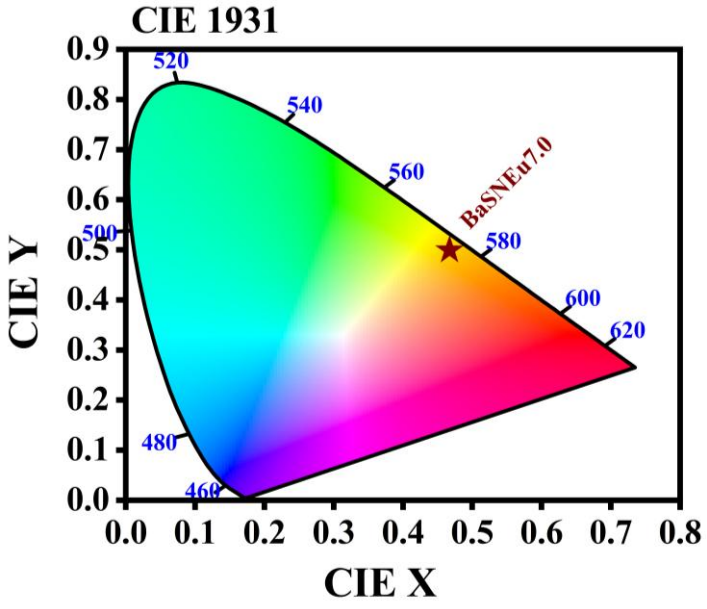

Figure 4.12: CIE chromaticity coordinate of Eu^{3+} ions 7.0 mol% concentration in BaSN phosphors

Table 3: The calculated CIE coordinates, color purity and CCT values for different concentration of Eu^{3+} ions doped BaSN phosphor

Activator ions concentration (Eu^{3+}) mol%	CIE Coordinates (x,y)	Colour Purity (% age)	CCT (Kelvins)
1.0	(0.40171, 0.5536)	80.88	4348
3.0	(0.47844, 0.4917)	92.15	3010
5.0	(0.49424, 0.4787)	89.88	2748
7.0	(0.4672, 0.49918)	89.51	3194
9.0	(0.48621, 0.48444)	90.82	2873

CONCLUSIONS AND FUTURE SCOPE

We successfully synthesized Eu^{3+}-doped $Ba_3SrNb_2O_9$ (BaSN) phosphors with varying Eu^{3+} concentration (1.0, 3.0, 5.0, 7.0 and 9.0 mol%) using the conventional solid-state method to study the various properties of the powdered samples such as their structure, morphology, and photoluminescence properties. The XRD spectra confirmed its high phase purity along with the formation of a single-phase hexagonal host lattice with the space group no. P63/m. The phase purity of the BaSN phosphor was verified when matched them with the standard JCPDS data, and the mean size of the crystal was lie in the range of 40-45 nm.

Further, SEM images revealed that the particles were in the micrometer range. The estimated the values of the optical band gap, using Tauc plots and were found to be between 4.27 and 4.51 eV, suggesting that these materials could be well-suited for solid-state lightning applications.

The Photoluminescence emissions were detected for the same phosphor under the near-UV excitation wavelength of 395 nm and most intense emission peak is observed at a wavelength of 592 nm corresponds to the $^5D_0$ to $^7F_2$ transition. The threshold for the optimum concentration for intense emission is 7.0 mol% of Eu^{3+} ions and beyond this concentration the decrease in emission intensity was monitored thus, quenching occurred. Photoluminescence analysis showed five main emission peaks at 364, 386, 395, 406 and 466 nm ascribed to the transitions originated from $^7F_0 \rightarrow {}^5D_4$, $^5G_2$, $^5L_6$, $^5D_3$ and $^5D_2$, respectively having the strongest emission at 592 nm.

We also observed that increasing the Eu^{3+} concentration led to a decline in emission intensity beyond 7.0 mol%, due to concentration quenching caused by dipole–dipole (d-d) interactions among the Eu^{3+} ions. The CIE coordinates (0.4672, 0.49918), calculated at 395 nm excitation, fall in the reddish-orange region, and the corresponding CCT values (2873 – 4348 K) suggest the phosphor is a good candidate for white LED applications.

The decay curves showed a bi-exponential pattern, with lifetime values ranging from 0.8 to 1.7 milliseconds, which decreased with higher Eu^{3+} concentrations due to energy transfer mechanism between the ions. Overall, Eu^{3+}-activated $Ba_3SrNb_2O_9$ phosphors demonstrate a promising potential for their application in the w-LEDs and photonic devices.

FUTURE SCOPE:

Additionally, detailed studies can be performed to evaluate whether co-doping with other activator ions further enhances luminescence intensity. The phosphor could be investigated further under both low and high-temperature conditions to study its thermal stability and reliability for practical applications. Also, there is substantial interest in extending its applicability to photonic devices and solid-state lighting systems, other than white light-emitting diodes (w-LEDs).